



Collision enhanced hyper-damping in nonlinear elastic metamaterial

Miao Yu(于淼), Xin Fang(方鑫), Dianlong Yu(郁殿龙), Jihong Wen(温激鸿), and Li Cheng(成利)

Citation: Chin. Phys. B, 2022, 31 (6): 064303. DOI: 10.1088/1674-1056/ac48fc

Journal homepage: <http://cpb.iphy.ac.cn>; <http://iopscience.iop.org/cpb>

What follows is a list of articles you may be interested in

Impact vibration properties of locally resonant fluid-conveying pipes

Bing Hu(胡兵), Fu-Lei Zhu(朱付磊), Dian-Long Yu(郁殿龙), Jiang-Wei Liu(刘江伟), Zhen-Fang Zhang(张振方), Jie Zhong(钟杰), and Ji-Hong Wen(温激鸿)

Chin. Phys. B, 2020, 29 (12): 124301. DOI: 10.1088/1674-1056/abb312

Using Helmholtz resonator arrays to improve dipole transmission efficiency in waveguide

Liwei Wang(王力维), Li Quan(全力), Feng Qian(钱枫), Xiaozhou Liu(刘晓宙)

Chin. Phys. B, 2019, 28 (9): 094301. DOI: 10.1088/1674-1056/ab3447

A novel multi-cavity Helmholtz muffler

Han-Bo Shao(邵瀚波), Huan He(何欢), Yan Chen(陈岩), Guo-Ping Chen(陈国平)

Chin. Phys. B, 2019, 28 (5): 054303. DOI: 10.1088/1674-1056/28/5/054303

Propagation of acoustic waves in a fluid-filled pipe with periodic elastic Helmholtz resonators

Dian-Long Yu(郁殿龙), Hui-Jie Shen(沈惠杰), Jiang-Wei Liu(刘江伟), Jian-Fei Yin(尹剑飞), Zhen-Fang Zhang(张振方), Ji-Hong Wen(温激鸿)

Chin. Phys. B, 2018, 27 (6): 064301. DOI: 10.1088/1674-1056/27/6/064301

Analysis of underwater decoupling properties of a locally resonant acoustic metamaterial coating

Ling-Zhi Huang(黄凌志), Yong Xiao(肖勇), Ji-Hong Wen(温激鸿), Hai-Bin Yang(杨海滨), Xi-Sen Wen(温熙森)

Chin. Phys. B, 2016, 25 (2): 024302. DOI: 10.1088/1674-1056/25/2/024302

Collision enhanced hyper-damping in nonlinear elastic metamaterial

Miao Yu(于淼)¹, Xin Fang(方鑫)^{1,2,†}, Dianlong Yu(郁殿龙)¹, Jihong Wen(温激鸿)¹, and Li Cheng(成利)²

¹Laboratory of Science and Technology on Integrated Logistics Support, National University of Defense Technology, Changsha 410073, China

²Department of Mechanical Engineering, Hong Kong Polytechnic University, Hong Kong, China

(Received 1 October 2021; revised manuscript received 29 December 2021; accepted manuscript online 29 December 2021)

Nonlinear elastic metamaterial, a topic which has attracted extensive attention in recent years, can enable broadband vibration reduction under relatively large amplitude. The combination of damping and strong nonlinearity in metamaterials may entail extraordinary effects and offer the capability for low-frequency and broadband vibration reduction. However, there exists a clear lack of proper design methods as well as the deficiency in understanding properties arising from this concept. To tackle this problem, this paper numerically demonstrates that the nonlinear elastic metamaterials, consisting of sandwich damping layers and collision resonators, can generate very robust hyper-damping effect, conducive to efficient and broadband vibration suppression. The collision-enhanced hyper damping is persistently presented in a large parameter space, ranging from small to large amplitudes, and for small and large damping coefficients. The achieved robust effects greatly enlarge the application scope of nonlinear metamaterials. We report the design concept, properties and mechanisms of the hyper-damping and its effect on vibration transmission. This paper reveals new properties offered by nonlinear elastic metamaterials, and offers a robust method for achieving efficient low-frequency and broadband vibration suppression.

Keywords: nonlinear elastic metamaterial, hyper-damping, vibration suppression

PACS: 43.40.+s

DOI: 10.1088/1674-1056/ac48fc

1. Introduction

In the last decade, elastic metamaterials have shown great promise for elastic wave manipulation,^[1–4] which are mainly limited to linear elastic metamaterials. In linear metamaterials, bandgaps arising from local resonances and Bragg scattering are of great significance for vibration reduction.^[5,6] Limited by the mass and the size in practice, commonly achieved low-frequency bandgaps usually exhibit narrow-band feature. Attaching different resonators^[7–10] or amplifying the inertia^[11–14] can broaden the bandgaps to a certain extent. Another important effect for vibration reduction and wave energy absorption in linear metamaterials is the hyper damping induced by local resonances.^[15–17] This means that a material processes superior dissipation ability as compared with other materials with the same damping composition and equivalent static properties.^[18] This is generally achieved by composite/architected materials or metamaterials. The hyper-damping effect in linear elastic metamaterials has been studied in a series of works by using different metamaterial configurations. Damping leads to broader vibration suppression, at the expenses of compromising the bandgaps. At present, realizing low-frequency and broadband bandgaps and simultaneous hyper damping remains a challenge in linear elastic metamaterials.^[19,20]

Elastic metamaterials with strong nonlinearity, i.e., nonlinear elastic metamaterials, can give rise to extraordinary physical phenomena, which can be exploited for elastic wave manipulation and vibration suppression.^[21–24] Therefore, non-

linear elastic metamaterial becomes a hot topic in recent years. Due to the high-order harmonics, wave energy in nonlinear elastic metamaterials can be transferred from low to higher frequencies.^[21,22] Except for the conventional band gaps similar to linear metamaterials, a region near 1/2-subharmonic in nonlinear elastic metamaterials can widen the frequency range of vibration attenuation.^[23,24] Nonlinear effects can produce tunable and adaptive band gaps.^[25–30] The amplitudes of nonlinear resonances in chaotic bands of nonlinear elastic metamaterials can be significantly suppressed, which greatly expands the bandwidth of suppressed waves.^[31–37] However, the desired nonlinear effect requires relatively large incident amplitude, whilst achievable nonlinear coefficient in practical structures is usually limited. Moreover, vibration transmission in nonlinear metamaterials remains high when the incident amplitude becomes very large.^[37] Damping and even hyper-damping effect may alleviate these challenges to improve the performance of nonlinear metamaterials. However, ways to achieve hyper damping in nonlinear elastic metamaterials are lacking and, even if achievable, the mechanisms underpinning the physical process remains unclear.

As well known, a viscous damper connecting two elements produces a damping force F_d , which is proportional to the relative velocity v between the two objects, namely $F_d = cv$, where v is the gradient of relative displacement. For a given damping coefficient c , introducing an abrupt change of displacement can increase v and F_d to produce large energy dissipation because the “abrupt change” leads to the infinite gradient in mathematics. A dedicated way for producing

[†]Corresponding author. E-mail: xinfangdr@sina.com

such an abrupt change is through the collision between the objects, which subsequently generates strong nonlinear damping forces. Capitalizing on this concept, we design a nonlinear elastic metamaterial by combining the damping and collision in a meta-cell, which can induce robust hyper damping as required. This paper aims at investigating the feasibility of such design, tackling a few important aspects relating to its materialization and shedding lights on the underlying mechanisms. More specifically, we numerically study the damping efficiency and vibration transmission of different metamaterial models. The influences of amplitude and damping coefficient are analyzed to find a robust design scheme. This paper offers a novel way for conceiving nonlinear elastic metamaterials which entail effective vibration suppression.

2. Model and methods

2.1. Metamaterial models

We consider a finite one-dimensional metamaterial model shown in Fig. 1. Each meta-cell consists of a primary mass m_0 , which is coupled to a resonator. Three kinds of coupling arrangement inside the meta-cell are considered, as shown in Figs. 1(b)–1(d). The damping in the primary chain is neglected. As a result, damping only comes from the motion inside meta-cells.

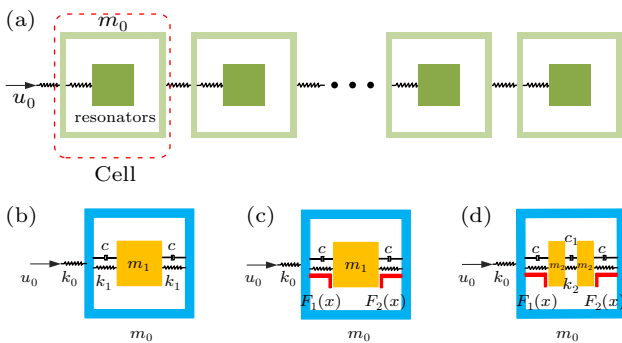


Fig. 1. Model of elastic metamaterial and its constituent meta-cell. (a) Elastic metamaterial model; (b) linear meta-cell; (c) meta-cell with bilateral collision; (d) sandwich-collision meta-cell.

The first coupling scenario depicted in Fig. 1(b) leads to a linear metamaterial. The equation of motion in the n^{th} cell writes

$$\begin{aligned} m_0 \ddot{u}_n &= k_0(u_{n+1} + u_{n-1} - 2u_n) \\ &\quad + 2k_1(y_n - u_n) + 2c_0(\dot{y}_n - \dot{u}_n), \\ m_1 \ddot{y}_n &= 2k_1(u_n - y_n) + 2c_0(\dot{u}_n - \dot{y}_n), \end{aligned} \quad (1)$$

where u_n and y_n are the displacement of the primary mass m_0 and the local resonator m_1 in the n^{th} cell, respectively, k_0 is the stiffness of the spring between neighbor m_0 , and k_1 is the linear stiffness between m_0 and m_1 . Here, a bilateral damping is introduced between m_0 and m_1 , and c_0 denotes the damping coefficient.

In the second model shown in Fig. 1(c), in addition to the linear stiffness k_1 , the bilateral collision of m_1 is introduced. According to the Hertz contact theory, the collision force takes the form of $k_N \delta^{3/2}$, where k_N is the collision stiffness. Therefore, expressions of forces F_1 and F_2 labeled in Fig. 1(c) write

$$F_1(x) = \begin{cases} k_1 x, & (x \geq -d), \\ k_1 x - k_N (-x - d)^{3/2}, & (x < -d), \end{cases} \quad (2)$$

$$F_2(x) = \begin{cases} k_1 x + k_N (x - d)^{3/2}, & (x > d), \\ k_1 x, & (x \leq d). \end{cases} \quad (3)$$

Here $d > 0$ denotes the clearance between m_1 and m_0 . Thus, the equations of motion of the n^{th} cell of the second nonlinear elastic metamaterial reads

$$\begin{aligned} m_0 \ddot{u}_n &= k_0(u_{n+1} + u_{n-1} - 2u_n) + F_1(y_n - u_n) \\ &\quad + F_2(y_n - u_n) + 2c_0(\dot{y}_n - \dot{u}_n), \\ m_1 \ddot{y}_n &= F_1(u_n - y_n) + F_2(u_n - y_n) + 2c_0(\dot{u}_n - \dot{y}_n). \end{aligned} \quad (4)$$

The third model shown in Fig. 1(d) also considers the collision nonlinearity, but the mass m_1 is split into two identical resonators, $m_2 = m_1/2$. Besides the nonlinear coupling between m_2 and m_0 , the damping and linear coupling between the two masses m_2 are also considered. We will show later that this tiny change leads to a significant improvement of the performance. The resulting metamaterial is referred to as sandwich-collision metamaterial because the damping between the two m_2 behaves like a sandwich cake. Similar to the second model, the equations of motion in the n^{th} cell of the third metamaterial write

$$\begin{aligned} m_0 \ddot{u}_n &= k_0(u_{n+1} + u_{n-1} - 2u_n) + F_1(y_{2n-1} - u_n) \\ &\quad + F_2(y_{2n} - u_n) + c_0(\dot{y}_{2n-1} - \dot{u}_n) + c_0(\dot{y}_{2n} - \dot{u}_n), \\ m_2 \ddot{y}_{2n-1} &= F_1(u_n - y_{2n-1}) + k_2(y_{2n} - y_{2n-1}) \\ &\quad + c_0(\dot{u}_n - \dot{y}_{2n-1}) + c_1(\dot{y}_{2n} - \dot{y}_{2n-1}), \\ m_2 \ddot{y}_{2n} &= F_2(u_n - y_{2n}) + k_2(y_{2n-1} - y_{2n}) \\ &\quad + c_0(\dot{u}_n - \dot{y}_{2n}) + c_1(\dot{y}_{2n-1} - \dot{y}_{2n}), \end{aligned} \quad (5)$$

where y_{2n-1} and y_{2n} are the displacements of the two resonators m_2 in the n^{th} cell, k_2 is the linear stiffness of the spring connecting the two resonators, and c_1 is the damping coefficient of the damper between them.

We note that the above three models have the same length of 12 cells. As shown in Fig. 1, in every model, the first meta-cell is subject to an incident wave source u_0 , and the last meta-cell is free. The incident displacement is expressed as $u_0 = A_0 \sin(\omega t)$ in which A_0 denotes the incident amplitude and $\omega = 2\pi f$ is the angle frequency. The frequency response of the elastic metamaterials can be obtained by solving the transmission of elastic metamaterial under different excitation frequencies f .

The parameters of elastic metamaterials with three different structures are set as follows: $m_0 = 0.1$ kg, $m_1 = 0.05$ kg, $k_0 = (2\pi \cdot 100)^2 \cdot m_0$ N/m, and $k_1 = (2\pi \cdot 20)^2 \cdot 0.25$ N/m. The parameters for collision oscillator are $k_N = 1 \times 10^{10}$ and $d = 0.0003$ m. In the third model, $m_2 = 0.025$ kg and $k_2 = (2\pi \cdot 20)^2 \cdot 0.25$ N/m. Other parameters are the same as collision elastic metamaterials. Unless otherwise specified as $c_0 = 1$ kg/s.

2.2. Numerical methods

We adopt the numerical integration approach to solve the time-domain response of these models. For mono-frequency input, the simulation time is 50 s, and the signal segment during 40 s–50 s is taken to calculate the transmission and damping properties. The simulation time is long enough for the system to reach a steady state. The transmission is quantified by $T = A_{\text{end}}/A_0$, where A_{end} is the average amplitude of the last m_0 in the chain

$$A_{\text{end}} = \left(\sum_{i=1}^M P_i - \sum_{j=1}^N V_j \right) / (M + N), \quad (6)$$

where P_i and V_j are the peak and valley (negative) values of the signal in 40 s–50 s, respectively. We note that collision may lead to chaotic response and this method gives an average amplitude.

2.3. Damping evaluation

To derive a rigorous metric to evaluate the damping in these high-dimensional systems, we shall first clarify the energy dissipation and transmission in the systems. Here we start with a single-degree-of-freedom linear system as illustrated in Fig. 2. The damping force on the mass m is $F = c \cdot v$ and its displacement is $u = A \sin(\omega t)$. In a period $2\pi/\omega$, the work done by the damping force reads

$$\begin{aligned} W &= \int_0^{2\pi/\omega} c \cdot \dot{u} \cdot \dot{u} dt \\ &= \int_0^{2\pi/\omega} c \cdot \omega^2 A^2 \cos^2(\omega t) dt \\ &= \pi \omega A^2 c. \end{aligned} \quad (7)$$

The maximum kinetic energy is

$$E_{\text{max}} = \frac{1}{2} \cdot v_{\text{max}}^2 m = \frac{1}{2} \cdot \omega^2 A^2 m. \quad (8)$$

The maximum potential energy is

$$U_{\text{max}} = \frac{1}{2} \cdot k A^2. \quad (9)$$

The damping effect can be evaluated by the index

$$\eta = W / \sqrt{E_{\text{max}} \cdot U_{\text{max}}} = 2\pi c / \sqrt{mk}, \quad (10)$$

where η is a dimensionless quantity that is independent of the frequency ω and the amplitude A . In engineering, the damping ratio is defined as $\zeta = c / (2\sqrt{mk})$ and $\zeta = 4\pi\eta$. Therefore, ζ is also a damping ratio.

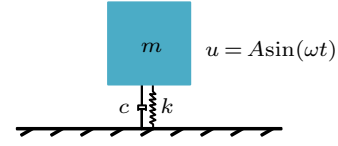


Fig. 2. Schematic diagram of simple harmonic motion of single degree of freedom system.

The metamaterials under investigation form a multiple-degrees-of-freedom system. The index for damping ratio should also reflect the wave transmission. Therefore, we adopt a similar expression like Eq. (10) to define the corresponding damping ratio as

$$\eta = W_m / \sqrt{E_{\text{max}}^{\text{end}} \cdot U_{\text{max}}^{\text{end}}}, \quad W_m = \sum_{i=1}^{N_{\text{cell}}} W_i / N_{\text{cell}}, \quad (11)$$

where $E_{\text{max}}^{\text{end}}$ and $U_{\text{max}}^{\text{end}}$ denote the maximum kinetic energy and potential energy of the last meta-cell, respectively. Moreover, W_i is the work done by damping in the i^{th} cell in a period of $2\pi/\omega$, and N_{cell} is the number of cells. For the finite metamaterial model, $N_{\text{cell}} = 12$; for the meta-cell model, $N_{\text{cell}} = 1$. Therefore, W_m is the average work done by the damping in all cells in a period of $2\pi/\omega$. For the first and the second metamaterial models,

$$W_i = \int_0^{T_{\text{sim}}} 2c_0 \cdot (\dot{u}_i - \dot{y}_i)^2 dt / (T_{\text{sim}} \cdot f). \quad (12)$$

For the third sandwich-collision elastic metamaterial,

$$\begin{aligned} W_i &= \int_0^{T_{\text{sim}}} [c_0 \cdot (\dot{u}_i - \dot{y}_{2i-1})^2 + c_0 \cdot (\dot{u}_i - \dot{y}_{2i})^2 \\ &\quad + c_1 \cdot (\dot{y}_{2i-1} - \dot{y}_{2i})^2] dt / (T_{\text{sim}} \cdot f), \end{aligned} \quad (13)$$

where T_{sim} is the simulation time.

2.4. Vibration and damping of a meta-cell model

Before systematically studying the properties of the metamaterials, we first investigate the general dynamics of a single meta-cell in this section.

The meta-cell is driven by a displacement $u_0 = A_0 \sin(\omega t)$. The frequency responses of the meta-cell, in terms of $T = A/A_0$ under variable excitation amplitudes A_0 , are shown in Fig. 3, where A is the average amplitude of the resonator m_0 . The frequency response of the first linear meta-cell is of course independent of A_0 . Its resonant frequencies are 20 Hz and 100 Hz. The first resonant peak is not obvious in this figure because of damping (see Fig. A1(a) in Appendix A).

For the second meta-cell (see Fig. 3(b)), no collision occurs when the vibration amplitude is smaller than the clearance d , on which occasion, its response is identical with the

linear cell. With increasing A_0 , collision takes place and its resonant peak $T = A/A_0$ gradually decreases. Near the critical $A_0 (= 5 \times 10^{-5} \text{ m in this case})$, the peak value of $T = A/A_0$ reaches minimal, i.e., the best parameter for vibration reduction in this system. Further increasing A_0 induces strong collision interaction between m_0 and m_1 . The resonant frequency is shifted to $(\sqrt{k_0/(m_0 + m_1)})/2\pi$, suggesting that the two resonators behave like a merged resonator with a total mass $m_0 + m_1$. However, this does not continuously reduce the resonant peaks. Instead, it increases significantly, indicating that the vibration deteriorates under extremely strong nonlinearity (when A_0 becomes excessively large).

In order to compare the damping in the third type of meta-cell, we consider two cases with weak damping. Case 1: $c_0 = 0 \text{ kg/s}$, $c_1 = 1 \text{ kg/s}$, and case 2: $c_0 = 1 \text{ kg/s}$, $c_1 = 1 \text{ kg/s}$. The corresponding frequency responses are shown in Figs. 3(c) and 3(d), respectively. In case 1, small A_0 produces similar phenomena as linear system. When increasing A_0 , though shifted, the resonant frequency does not reach $(\sqrt{k_0/(m_0 + m_1)})/2\pi$ as the second model does. Its frequency response peak will also gradually decrease. When further increasing A_0 , more branches and peaks are generated in the vicinity of the main resonant peak. Fortunately, the value of the main peak will not rise significantly. In this case, m_0 and m_2 move in phase but not synchronized, the displacement of the two m_2 in their non-collision direction is greater than that of the m_0 (see

Fig. B1(d)). For case 2, the variation trend of the frequency response with A_0 is similar to that of case 1, with however, a much reduced peak value for $A_0 > 1 \times 10^{-4} \text{ m}$.

Furthermore, we use the damping ratio ζ to evaluate the energy dissipation ability in the meta-cell model, as shown in Fig. 4. For the first linear meta-cell, the ratio ζ depends on frequency and is independent of A_0 . The peak value is always located at the resonant frequency at 20 Hz.

For the collision meta-cell, ζ depends on both frequency and A_0 . When A_0 is very small, the ratio ζ of the cell becomes large at the two resonance frequencies, and ζ at the resonance 20 Hz is much higher than at the other frequency 100 Hz. For $A_0 < 1 \times 10^{-4} \text{ m}$, ζ near 100 Hz increases lightly while increasing A_0 . For $A_0 > 1 \times 10^{-4} \text{ m}$, as m_0 and m_1 move synchronously (see Fig. B1(b)), ζ at both resonances gradually decreases.

For case 1 in the sandwich-collision meta-cell, ζ at the resonance frequency 100 Hz is large for small A_0 . While increasing A_0 , ζ at both 20 Hz and 100 Hz increases gradually, and a very broad band covering 20 Hz–250 Hz for the large damping ratio is generated, which indicates that the damping effect induced by sandwich-collision is very broadband. The variation trends in case 2 are similar with that in case 1, except that the damping ratio is much larger even for small input amplitude.

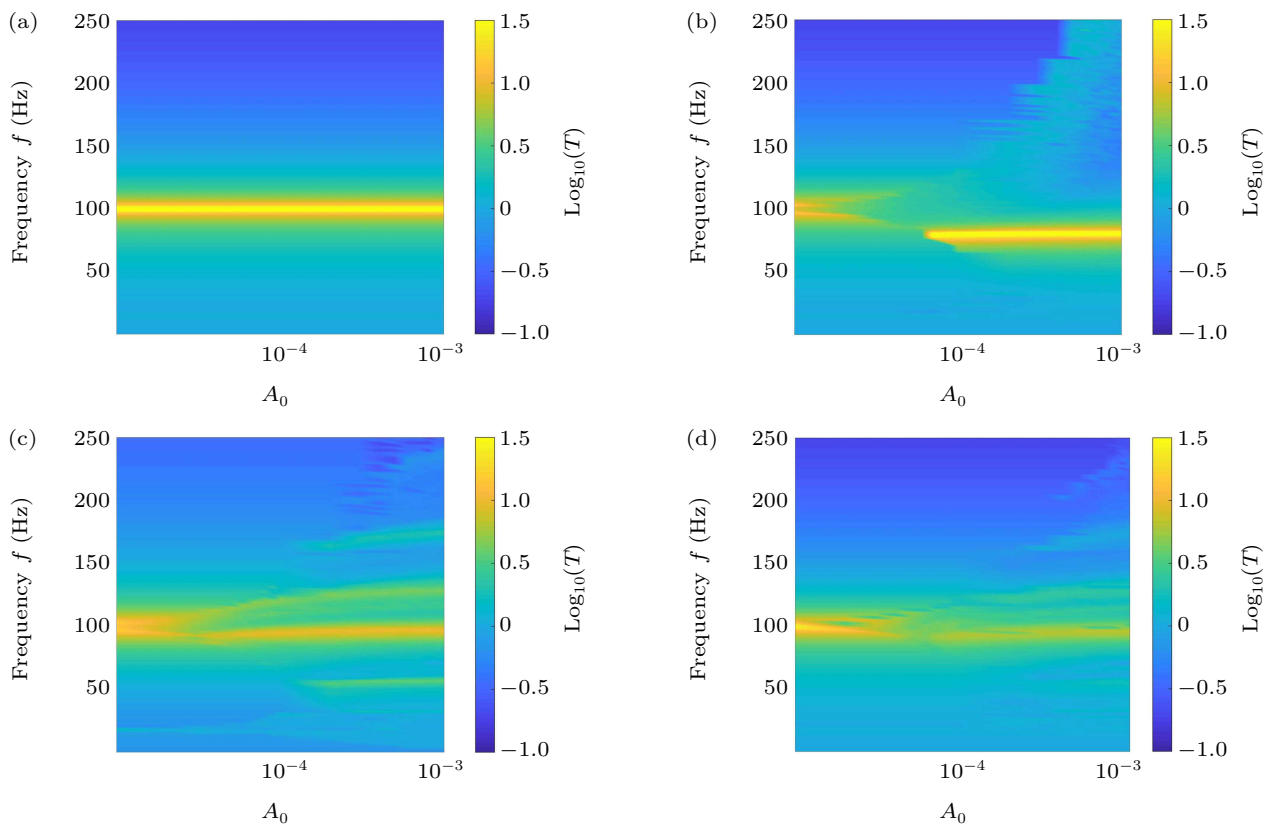


Fig. 3. Frequency response of meta-cells under different excitation amplitudes. (a) Linear meta-cell; (b) meta-cell with bilateral collision; (c) case 1 in sandwich collision meta-cell; (d) case 2 in sandwich collision meta-cell.

Moreover, we calculate the average damping ratio ζ_m and the average transmission T_m from 1 Hz–200 Hz to evaluate low-frequency properties. Interestingly, ζ_m and T_m are highly correlated and vary oppositely. For the specific parameters, $\zeta_m = 0.1$ and $T_m = 2.72$ are used for the linear meta-cell model. As shown in Fig. 4(f), when $A_0 < 10^{-4}$ m, T_m of all nonlinear models are smaller than that of the linear model. However, further increasing A_0 when $A_0 > 6 \times 10^{-5}$ m (the red circle in Fig. 4(f)), ζ_m of the second model with collision reduces to a tiny value, and T_m rapidly increases and becomes larger than that of the linear model. This suggests that a proper strength of nonlinearity can reduce the vibration of the system but an excessively strong nonlinearity will jeopardize the vibration reduction in the system.

As shown in Figs. 4(e) and 4(f), T_m of the third sandwich-collision model remains at the valley for both cases 1 and 2

and ζ_m increases to 0.36 and 0.7 in cases 1 and 2 respectively, much higher than the linear model. This means that the desired hyper damping appears owing to the damping between the two resonators m_2 in the sandwich-collision nonlinear model. Moreover, as $c_0 = 0$ kg/s in case 1 and $c_0 = 1$ kg/s in case 2, the damping between m_0 and m_2 doubles the whole hyper damping ratio ζ_m from 0.36 to 0.7, alongside a simultaneous reduction in the average transmission T_m from 2.0 to 1.55. This also signifies that the location of the damping layer would greatly influence the system property and the hyper damping is achieved.

The aforementioned analyses based on a meta-cell model show that tactic designing the strongly nonlinear model with sandwich-collision can produce hyper damping for efficient vibration reduction even under very large amplitude.

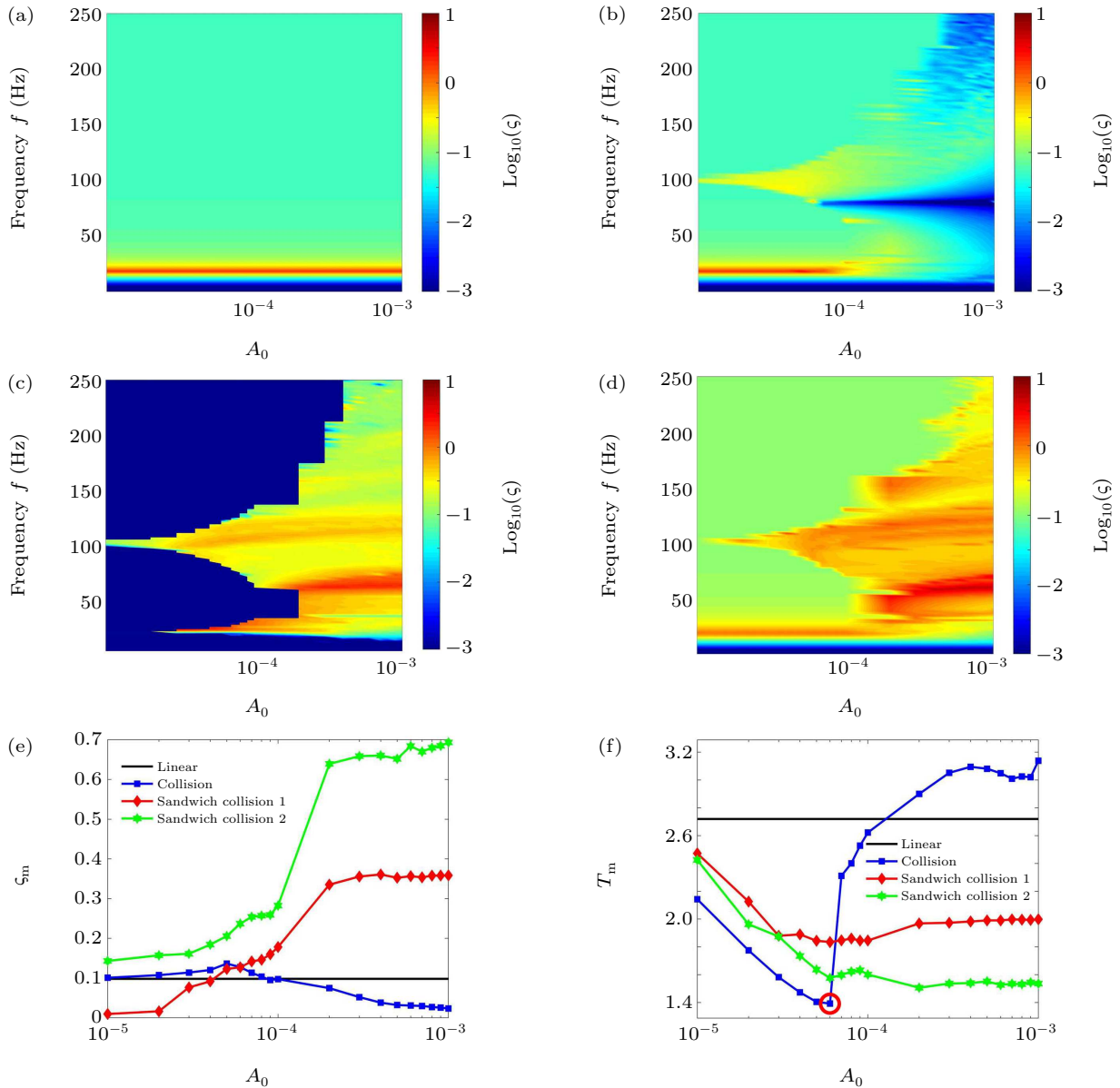


Fig. 4. Damping ratio ζ (a)–(d), average ratio ζ_m (e) and average transmission T_m (f) of meta-cells under different excitation amplitudes. (a) Linear meta-cell; (b) collision meta-cell; (c) sandwich-collision meta-cell 1; (d) sandwich-collision meta-cell 2; (e) average ratio ζ_m in four meta-cells; (f) average transmission T_m in four meta-cells.

3. Vibration and damping of metamaterials

In this section, we analyze the vibration and damping in the three types of elastic metamaterials with weak damping, $c_0 = 0$ or 1 kg/s and $c_1 = 1$ kg/s. Cases involving stronger damping are studied in the next section. The elastic metamaterials have very different properties from the meta-cell model. They have bandgaps and dense resonances in the passbands.

3.1. Bandgaps

Firstly, the dispersion curves in linearized metamaterials are calculated by using the periodic boundary conditions determined by Bloch theorem. Here only linear case is considered. For the diatomic model shown in Figs. 1(b) and 1(c), the dispersion equation writes

$$\cos(\kappa a) = 1 + \frac{m_0 m_1 \omega^4 - (m_0 + m_1) 2k_1 \omega^2}{2k_0(2k_1 - m_1 \omega^2)}, \quad (14)$$

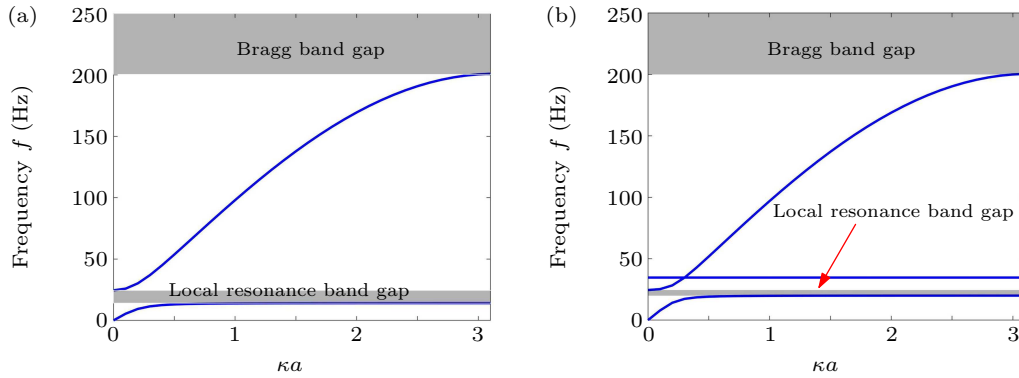


Fig. 5. Dispersion curves in linearized metamaterials. (a) Dispersion curves corresponding to Figs. 1(a) and 1(b) without collision. (b) Dispersion curves corresponding to Fig. 1(c) without collision.

3.2. Vibration transmission and damping

For the linear metamaterial, as shown in Fig. 6(a), the transmission within the band gap is of course much lower than that in the pass band, and its frequency response is independent of A_0 . As shown in Fig. 6(b), the peak value of ζ is always located at the band gaps, because the bandgaps prohibit wave propagation, which can be regarded as the equivalent large damping effect.

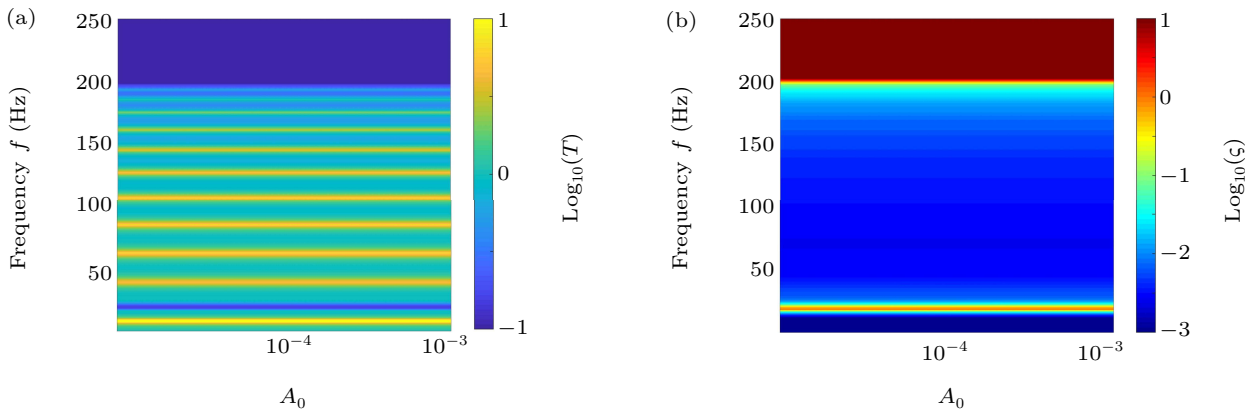


Fig. 6. Frequency response and ratio ζ of linear metamaterials. (a) Frequency response, (b) ratio ζ .

where $\kappa \in [\pi/a]$ is the wave vector, and a is the lattice constant.

The dispersion relationship of the model in Fig. 1(d) is

$$\cos(\kappa a) = 1 + \frac{m_0 m_2 \omega^4 - (k_1 m_0 + k_2 m_0 + 2k_1 m_2) \omega^2 + 2k_1 k_2}{2k_0(k_1 - m_1 \omega^2)}. \quad (15)$$

As shown in Fig. 5(a), the diatomic linear metamaterial has a locally resonant bandgap in 14.07 Hz–24.49 Hz, and a Bragg bandgap above 200 Hz. For the sandwich metamaterial in Fig. 5(b), there are also a narrower locally resonant bandgap in 19.94 Hz–24.49 Hz, and a Bragg bandgap above 200 Hz. Moreover, there is a straight line in Fig. 5(b), corresponding to $\omega = \sqrt{(k_1 + 2k_2)/m_2}$ because the second term in Eq. (15) is zero and $\cos(\kappa a) \equiv 1$ at this frequency.

For the second collision metamaterial, as shown in Fig. 7(a), its transmission in the whole passbands becomes minimal near $A_0 = 1 \times 10^{-4}$ m, like the property observed for the meta-cell. Moreover, the damping ratio of the whole band also become larger near $A_0 = 1 \times 10^{-4}$ m. However, the wave transmission (the damping ratio) is large (small) for both small and large amplitude, i.e., nonideal performance for vibration suppression.

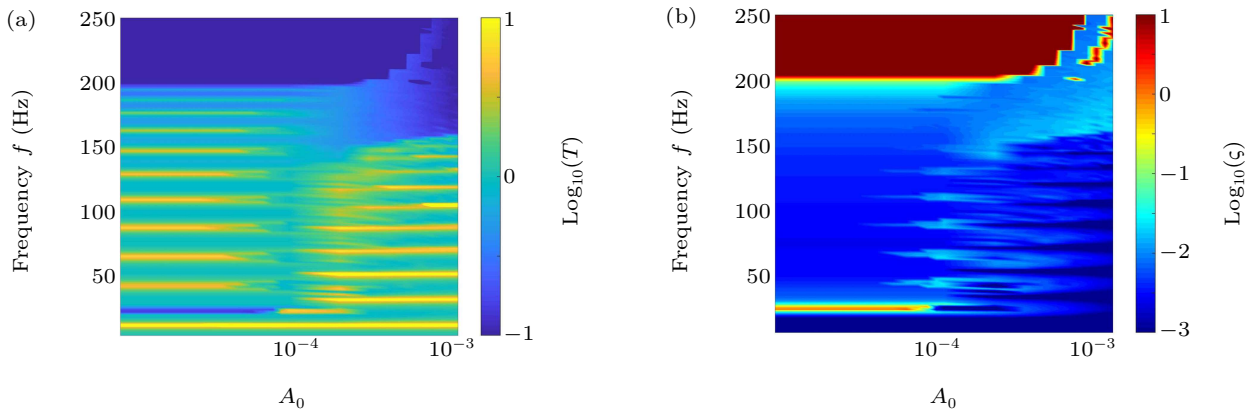


Fig. 7. Frequency response and ratio ζ of collision metamaterials. (a) Frequency response, (b) ratio ζ .

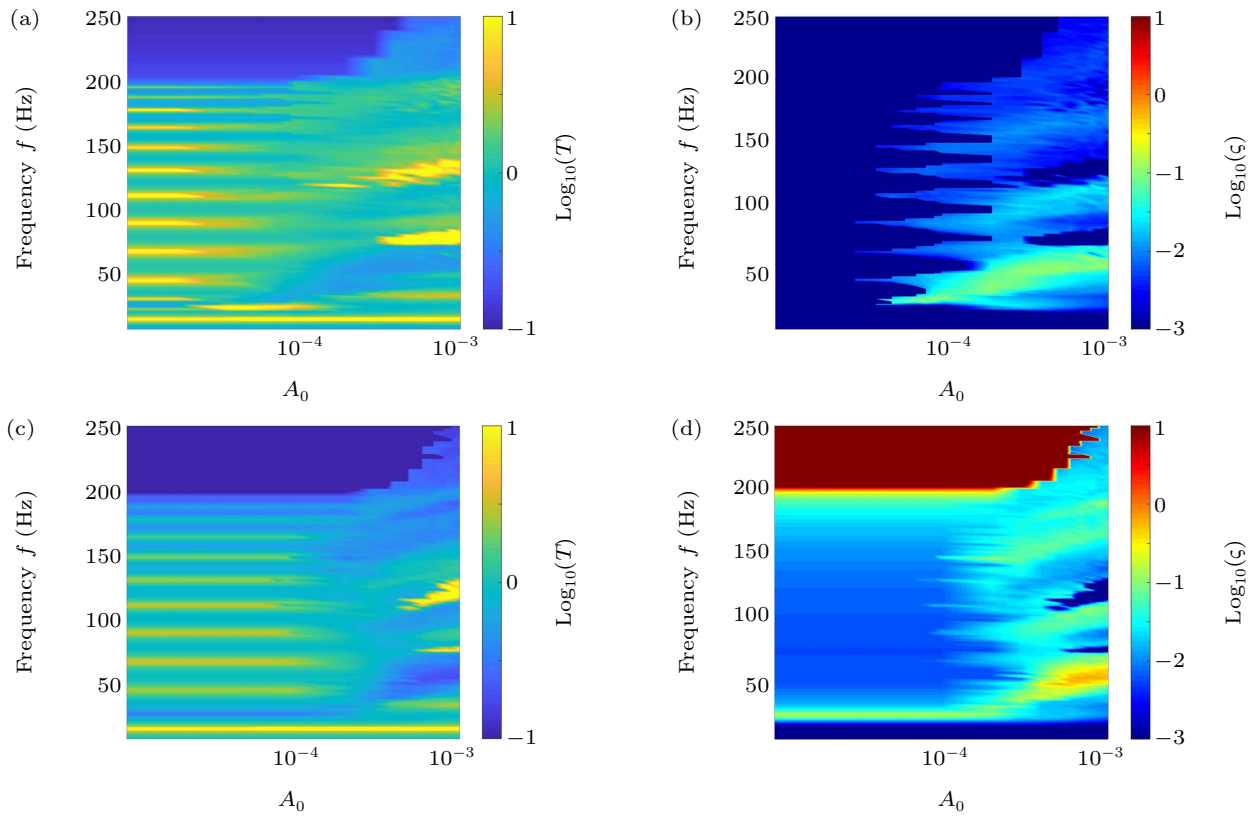


Fig. 8. Frequency response and ratio ζ of sandwich-collision metamaterials under different excitation amplitudes. (a) Frequency response of case 1, (b) ratio ζ of case 1, (c) frequency response of case 2, (d) ratio ζ of case 2.

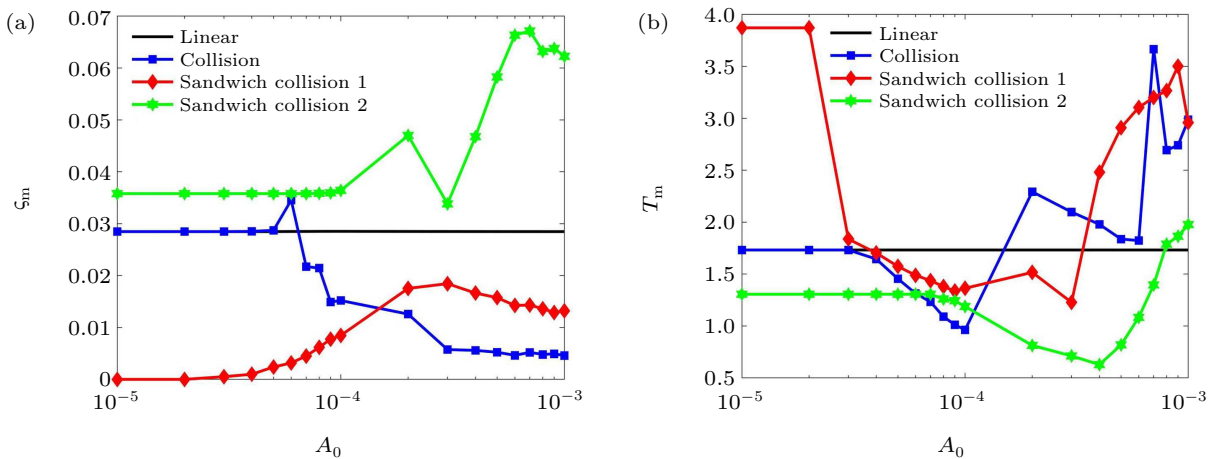


Fig. 9. Average ratio ζ_m (a) and average transmission T_m (b) of meta-cells in metamaterials under different excitation amplitudes.

Properties for the sandwich-collision metamaterial are shown in Fig. 8. As $c = 0$ in case 1, energy dissipation is only due to the relative motion between the two m_2 . However, as the two resonators are identical, their motions are synchronous in the ideal linear case, which means the defined damping ratio is zero. Therefore, the damping ratio in Fig. 8(b) is tiny under small amplitude, on which occasion, collision does not happen. Fortunately, when increasing the incident amplitude for $A_0 > 3 \times 10^{-5}$ m, collision between m_0 and m_2 takes place, the synchronous motion is then broken and the damping is active. The damping ratio increases with A_0 in this case within a very broadband. This evidences the collision-enhanced damping, directly responsible for the reduction in the vibration transmission in 20 Hz–200 Hz for case 2, and Figs. 8(c) and 8(d) shows similar properties with the linear metamaterial when A_0 is very small. When $A_0 > 1 \times 10^{-4}$ m, ζ significantly increases with A_0 due to the collision enhanced damping alongside a simultaneous reduction in the vibration.

Furthermore, we evaluate the average damping ratio ζ_m and the average transmission T_m in 1 Hz–200 Hz of these metamaterial models, as shown in Fig. 9. Their trends about the average damping ratio ζ_m and average transmission T_m changing with A_0 are similar to their meta-cell's. And we can see that in nonlinear metamaterials the damping ratio for relatively high amplitude (with collision nonlinearity) is much higher than that for small amplitude, which exhibits the broadband hyper damping property responsible for vibration reduction. It is obvious that such hyper damping is enhanced by the collision.

4. Influences of damping on the nonlinear sandwich-collision elastic metamaterial

In this section, we clarify the effects of damping c_0 and c_1 on the vibration transmission of nonlinear metamaterials. We numerically calculate the average transmission T_m in 20 Hz–200 Hz by changing both A_0 and the damping coefficients.

As there are multiple variables, the simulation with mono-frequency input, $u_0 = A_0 \sin(\omega t)$, is quite time-consuming to obtain the overall trends. Instead, we input the sweep-sine signal from 20 Hz–200 Hz within 200 s. The low sweeping speed used is to ensure that the responses obtained is very close to steady. The transmission spectrum $T(f)$ is obtained with fast Fourier transform.

For the second nonlinear metamaterial model with bilateral collision (see Fig. 10(a)), the average transmission T_m is always large for $c_0 < 4$ kg/s and increasing c_0 can open a parameter space (c_0, A_0) for $T_m < 1$ (i.e., 0 dB). There is an optimal range for c_0 to generate a minimal T_m . However, T_m always becomes large under larger incident amplitude A_0 .

For the third sandwich-collision model, we first study the influences of A_0 and c_0 under weak damping between the two local resonators $c_1 = 1$ kg/s (see Fig. 10(b)), and then study the influences A_0 and c_1 for weak damping between m_0 and m_2 , $c_0 = 1$ kg/s (see Fig. 10(c)). It is interesting that this metamaterial model has much larger parameter space (c_0, c_1 , and A_0) for $T_m < 1$ than the first model, which greatly improves the robustness in practice. Moreover, there is an optimal value of c_0 ($= 11$ kg/s here) for the minimal T_m in the first case with $c_1 = 1$ kg/s. Unusually, T_m becomes large again for strong damping c_0 in the first case. This trend also happens in the former nonlinear model shown in Fig. 10(a). This means that one still has to optimize the damping layer between m_0 and the inner resonators in practice. Fortunately, the trends in Fig. 10(c) show that the metamaterial with sandwich-collision is insensitive to c_1 , highlighting a robust feature.

It is well known, the phase diagram of the steady-state response of a linear damping system under single frequency excitation is a standard ring, as shown in Fig. 10(i). Figure 10(h) stands for a quasi-periodic state which consists of several superimposed rings. While the phase diagrams of Figs. 10(d)–10(g) can not form one or several rings as Figs. 10(h) and 10(i), which show the chaotic property.

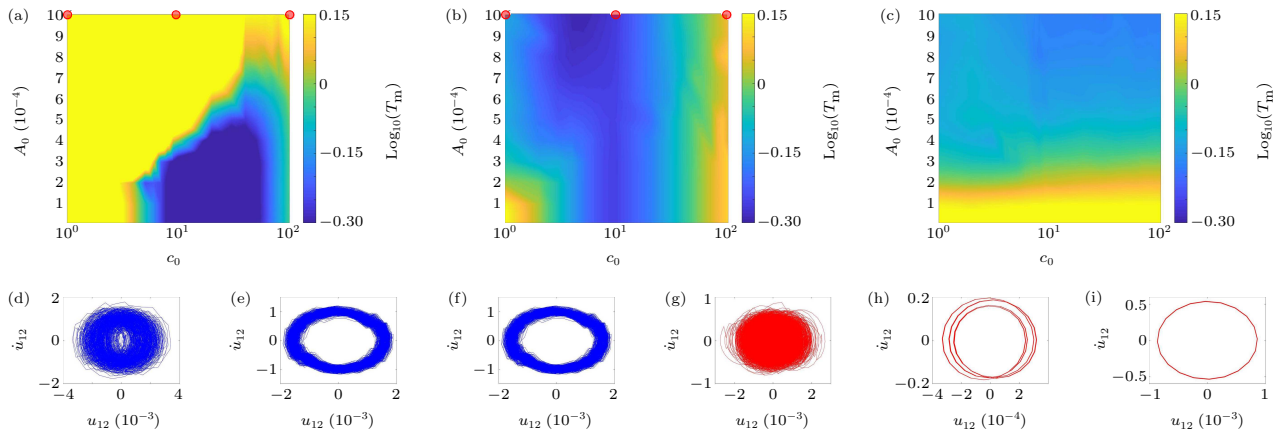


Fig. 10. Average transmission T_m of collision metamaterials and sandwich collision metamaterials with different c_0 and c_1 . Also with the phase diagram of the 12th meta-cell marked in (a) and (b). (a) Average transmission T_m of collision metamaterials with different c_0 . (b) Average transmission T_m of sandwich-collision metamaterials with different c_0 , in which $c_1 = 1$. (c) Average transmission T_m of sandwich-collision metamaterials with different c_1 , in which $c_0 = 1$. (d)–(i) Phase diagram obtained by single frequency excitation corresponding to the points marked in (a) and (b), the frequency of excitation is 100 Hz.

In short, the nonlinear metamaterial with sandwich collision can efficiently suppress low-frequency and broadband vibration, and meanwhile features strong robustness for varying or uncertain amplitude and damping.

5. Conclusion

This paper proposes the design of a hyper-damping nonlinear elastic metamaterial for efficient, robust, low-frequency and broadband vibration reduction, along with a systematic analysis of underlying mechanism and the effects of major system parameters. To this end, we study the properties of the nonlinear elastic metamaterial consisting of sandwich damping layers and collision resonators. The vibration transmission and damping ratio of three kinds of metamaterials, and the dynamics of a unit cell are numerically studied. We find that the hyper damping can be induced and enhanced by the collision in meta-cells, consisting of resonators coupled as a sandwich structure. The sandwich collision elastic metamaterial possesses a large parameter space (amplitude, damping, frequency), whose effective tuning can warrant efficient low-frequency and broadband vibration reduction through wave manipulation.

In conclusion, this paper, through tactic structural design, reveals new properties and possibilities that can be offered by nonlinear elastic metamaterials. Hopefully, it can offer new impetus to the grooming area of nonlinear metamaterial design and offers a novel and robust method for achieving efficient low-frequency and broadband vibration suppression.

Acknowledgments

Project supported by the National Natural Science Foundation of China (Grant Nos. 11872371, 11991032, and 12002371) and the Science and Technology Innovation Program of Hunan Province, China (Grant No. 2020RC4022).

Appendix A: Frequency responses of meta-cells

As shown in Fig. A1(a), by comparing frequency responses of linear meta-cell with damping ($c_0 = 1$) and without damping ($c_0 = 0$), we can see that the low-frequency peak is not obvious when there is relatively large damping. As shown in Figs. A1(b)–A1(d), for nonlinear meta-cell, frequency responses change with excitation amplitudes, and there is an optimal excitation amplitude range for vibration suppression.

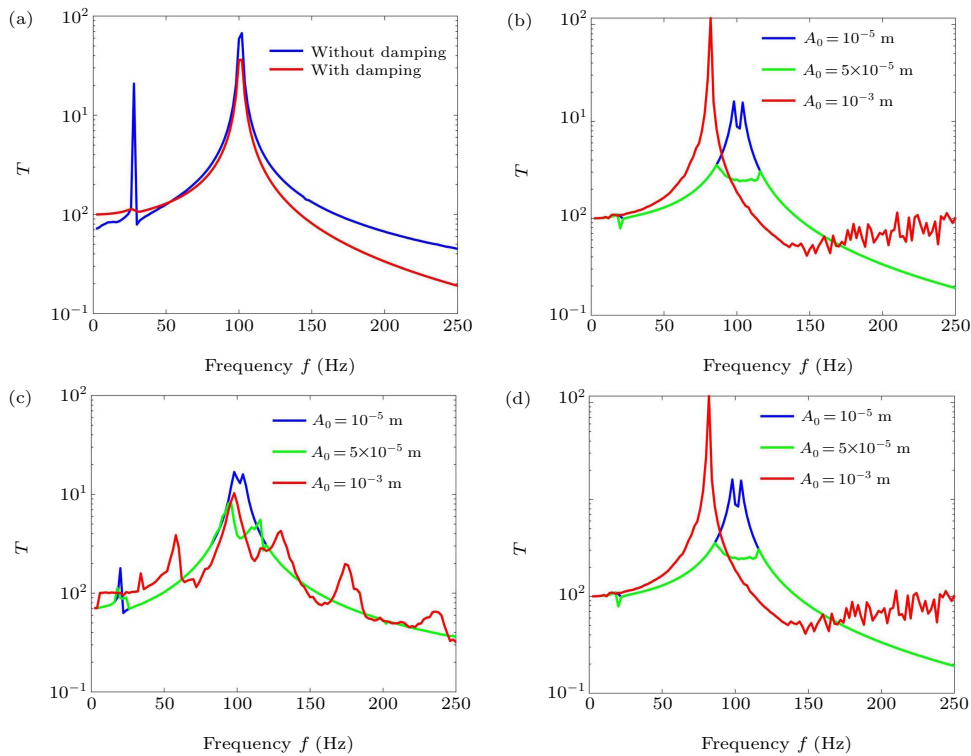


Fig. A1. Frequency response of linear meta-cell with and without damping, and nonlinear meta-cells under different excitation amplitudes. (a) Linear meta-cell; (b) collision meta-cell; (c) sandwich collision meta-cell 1; (d) sandwich collision meta-cell 2.

Appendix B: Time-domain diagrams of the meta-cells

As shown in Figs. B1(a) and B1(c), when the amplitude of excitation is small, m_0 and m_1 or m_2 move in opposite phase for collision and sandwich collision meta-cell. With amplitude

of excitation increasing, m_0 and m_1 move synchronously for collision meta-cell, as shown in Fig. B1(b). While for sandwich collision meta-cell 1, m_0 and m_2 move in the same phase but not synchronized, the displacement of the two m_2 in their non-collision direction is greater than that of the m_0 .

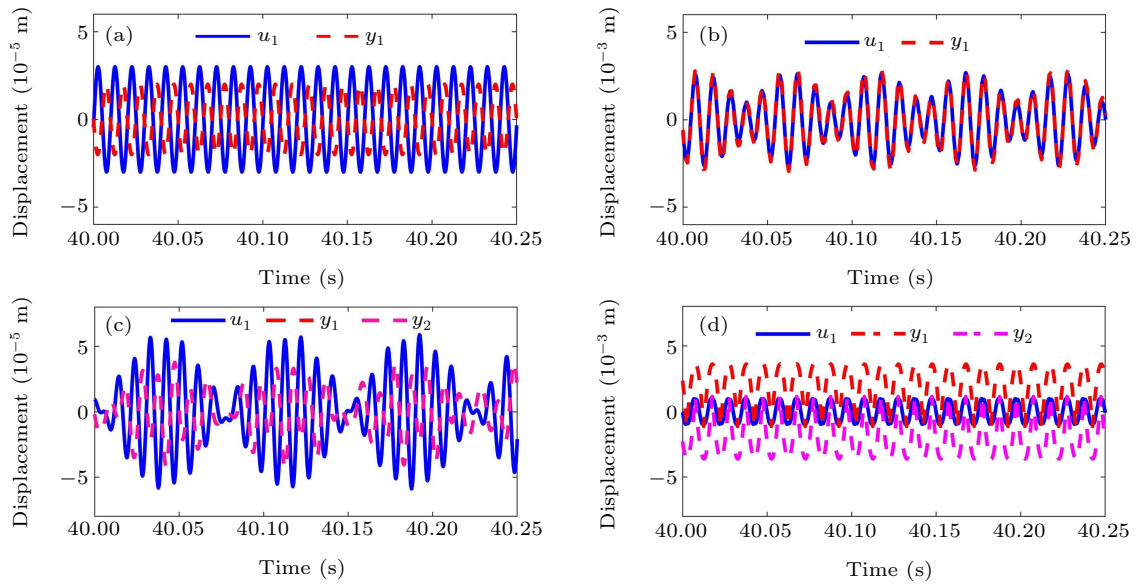


Fig. B1. Time domain responses of meta-cells, the frequency of excitation is 100 Hz. (a) Collision meta-cell when $A_0 = 10^{-5}$ m. (b) Collision meta-cell when $A_0 = 10^{-3}$ m. (c) Sandwich collision matecell 1 when $A_0 = 10^{-5}$ m. (d) Sandwich collision matecell 1 when $A_0 = 10^{-3}$ m.

Appendix C: Frequency responses of metamaterial models

As shown in Fig. C1, we can conclude that the frequency response of linear metamaterial model is independent of excitation amplitude and there is also an optimal excitation amplitude range for vibration suppression.

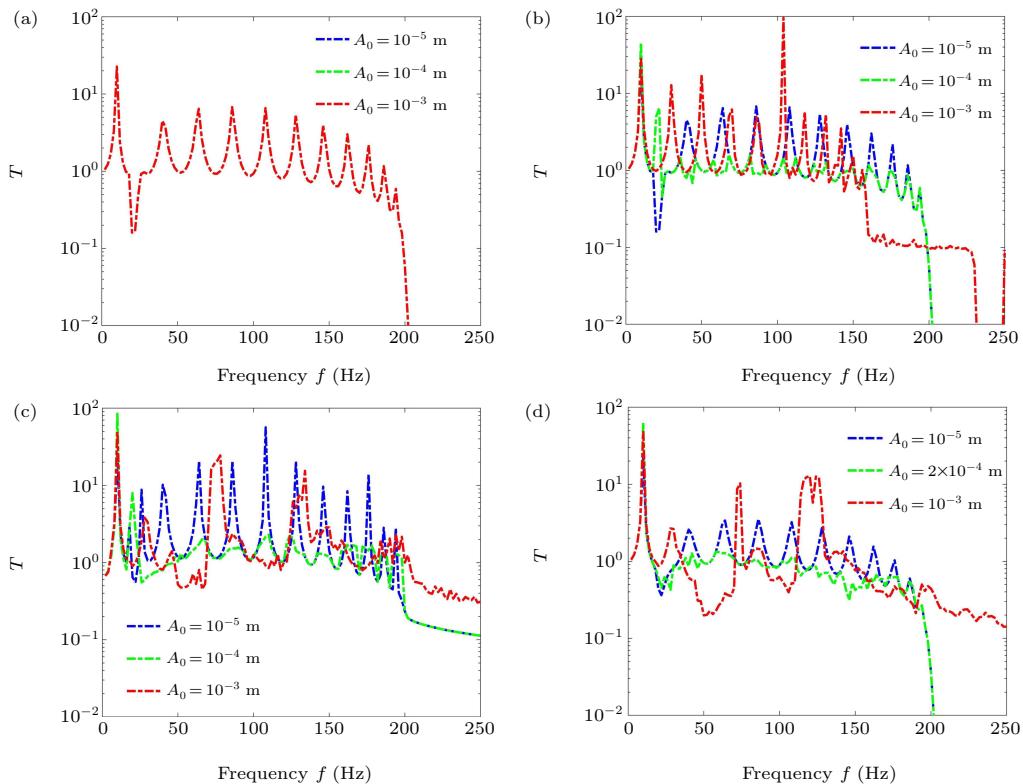


Fig. C1. Frequency response of metamaterial under different excitation amplitudes. (a) Linea metamaterial. (b) Collision metamaterial. (c) Sandwich collision metamaterial 1. (d) Sandwich collision metamaterial 2.

References

[1] Liu Z Y, Zhang X, Mao Y, Zhu Y Y, Yang Z, Chan C T and Sheng P 2000 *Science* **289** 1734
 [2] Ma G and Sheng P 2016 *Sci. Adv.* **2** e1501595
 [3] Liu J, Guo H and Wang T 2020 *Crystals* **10** 305
 [4] Kumar S and Lee H P 2020 *Crystals* **10** 686
 [5] Choi C, Bansal S, Münzenrieder N and Subramanian S 2021 *Adv. Eng. Mater.* **23** 2000988
 [6] Hussein M I, Leamy M J and Ruzzene M 2014 *Appl. Mech. Rev.* **66** 4
 [7] Yang C and Cheng L 2016 *J. Acoust. Soc. Am.* **139** 2361
 [8] Sugino C, Leademham S, Ruzzene M and Erturk A 2016 *J. Appl. Phys.* **120** 134501

- [9] Celli P, Yousefzadeh B, Daraio C and Gonella S 2019 *Appl. Phys. Lett.* **114** 091903
- [10] Yan Z Y and Wu J H 2017 *J. Phys. D Appl. Phys.* **50** 355104
- [11] Miniaci M, Mazzotti M, Amendola A and Fraternali F 2021 *Int. J. Solids. Struct.* **216** 156
- [12] Madhamshetty K and Manimala J M 2019 *J. Franklin. Inst.* **356** 7731
- [13] Zhou J, Dou L, Wang K, Xu D and Ouyang H 2019 *Nonlinear Dyn.* **96** 647
- [14] Al Ba'ba'a H, DePauw D, Singh T and Nouh M 2018 *J. Appl. Phys.* **123** 105106
- [15] Chen Y Y, Barnhart M V, Chen J K, Hu G K, Sun C T and Huang G L 2016 *Compos. Struct.* **136** 358
- [16] DePauw D, Al Ba'ba'a H and Nouh M 2018 *Extreme. Mech. Lett.* **18** 36
- [17] Aladwani A and Nouh M 2010 *Int. J. Mech. Sci.* **173** 105459
- [18] Hussein M I and Frazier M J 2013 *J. Sound Vib.* **332** 4767
- [19] Bacquet C L, Al Ba'ba'a H, Frazier M J, Nouh M and Hussein M I 2018 *Adv. Appl. Mech.* **51** 115
- [20] Frazier M J and Hussein M I 2012 *Proc. SPIE* **8348** 56
- [21] Mohammad, Bukhari and Oumar 2020 *Nonlinear Dyn.* **99** 1539
- [22] Manimala J M, Kulkarni P P and Madhamshetty K 2018 *Adv. Compos. Hybrid. Mater.* **1** 797
- [23] Silva P B, Leamy M J, Geers M G D and Kouznetsova V G 2019 *Phys. Rev. E* **99** 063003
- [24] Zega V, Silva P B, Geers M G D and Kouznetsova V G 2020 *Sci. Rep.* **10** 12041
- [25] Pajunen K, Celli P and Daraio C 2021 *Extreme. Mech. Lett.* **44** 101236
- [26] Emerson T A and Manimala J M 2020 *Acta Mech.* **231** 4665
- [27] Konarski S G, Haberman M R and Hamilton M F 2018 *J. Acoust. Soc. Am.* **144** 3022
- [28] Valappil S V, Sheehan C and Manimala J M 2018 *Proc. ASME Conf. Smart. Mater. Adapt. Struct. Intell. Syst.* **2018** 7932
- [29] Liu X, Cai G and Wang K W 2021 *J. Appl. Phys.* **129** 114902
- [30] Goldsberry B M and Haberman M R 2018 *J. Appl. Phys.* **123** 091711
- [31] Fang X, Wen J, Yin J, Yu D and Xiao Y 2017 *New J. Phys.* **19** 053007
- [32] Fang X, Wen J, Yin J, Yu D and Xiao Y 2016 *Phys. Rev. E* **94** 052206
- [33] Fang X, Wen J, Bonello B, Yin J and Yu D Y 2017 *Nat. Commun.* **8** 1
- [34] Fang X, Wen J, Yu D and Yin J 2018 *Phys. Rev. Appl.* **10** 054049
- [35] Fang X, Wen J, Benisty H and Yu D 2020 *Phys. Rev. B* **101** 104304
- [36] Fang X, Wen J, Yu D and Yin J 2018 *New J. Phys.* **20** 123028
- [37] Sheng P, Fang X, Wen J and Yu D 2021 *J. Sound Vib.* **492** 115739